DIMENSIONAL STABILITY OF COMPLEX SHAPES MANUFACTURED BY THE VARTM PROCESS

Pascal Hubert, Old Dominion University, Hampton, VA
Brian W. Grimsley, NASA Langley Research Center, Hampton, VA
Roberto J. Cano, NASA Langley Research Center, Hampton, VA
R. Byron Pipes, The University of Akron, Akron, OH

Abstract

The vacuum assisted resin transfer molding (VARTM) process is a cost effective, innovative method that is being considered for manufacture of large aircraft-quality components where high mechanical properties and dimensional tolerance are essential. In the present work, carbon fiber SAERTEX fabric/SI-ZG-5A epoxy resin C-shaped laminates were manufactured by VARTM using different cure cycles followed by the same post-cure cycle. The final part thickness was uniform except at the corner were thinning was observed. The cure cycle selected is shown to significantly affect the part spring-in and a long cycle at 66°C followed by a 178°C post-cure produced a part with negligible spring-in.

Introduction

Vacuum assisted resin transfer molding (VARTM) is a low cost manufacturing process primarily used in the boating industry to make boat hulls and other large structures. More recently, this manufacturing technique was used to make large aircraft components (1) such as vertical rudders and complex geometry parts found in missile fabrication (2). Cost reduction is a major benefit of using VARTM over conventional composite processes like autoclave curing. For example, it was estimated that using VARTM to make a complex component reduced the number of parts from 61 to one and eliminated more than 376 fasteners (2). Consequently, using VARTM resulted in a cost reduction of 75% over a conventional metal design while the component weight was the same and the performance was higher.

One of the critical issues for aerospace applications is the control of the component dimensions. Components must be assembled and therefore accurate prediction and control in part-to-part variation must be achieved. Dimensional control is achieved during the component processing cycle, thus it is important to have a good fundamental understanding of the process. For VARTM, the analysis of the part infiltration process has been the subject of an increasing number of studies (3-6). Analytical and numerical tools were developed to predict flow front position, part thickness change and local fiber volume fraction. However, the dimensional stability after cure of parts manufactured by VARTM has not been widely addressed. It is well known that the curing process induces residual stresses that cause part distortions and/or microcracks. These residual stresses are caused by several factors including thermal effects, cure shrinkage and tool-part interaction (7). Analysis of the spring-in of C-shaped laminates cured by the autoclave process revealed that the net measured spring-in angle was a combination of warpage and corner spring-in. The warpage was found to depend on the tool preparation leading to different tool-part interactions. The corner spring-in was caused by the difference between the longitudinal and transverse coefficient of thermal expansion (CTE) and resin cure shrinkage. The latter is a well known phenomenon when manufacturing anisotropic materials in curved parts (8,9).

In this work, the dimensional stability of C-shaped laminates manufactured by the VARTM process was studied. Different curing strategies were used to identify critical parameters particular to the VARTM process. The results obtained will allow one to understand how to control more precisely the geometry of components made by VARTM.

Experiments[1]

Composite C-shaped laminates were fabricated by the VARTM process using SAERTEX® multi-axial, non-crimp carbon fiber fabric and the A.T.A.R.D. SI-ZG-5A epoxy resin. The laminates contained two stacks of fabric resulting in a [45,-45,0,90,0,-45,45]s ply sequence. A 12.5 cm thick aluminum rectangular tube was used as a rigid tool surface (Figure 1a). The tool had outside dimensions of 10.2 cm x 15.0 cm with a radius of 0.6 cm on the corners.

---

[1] Use of trade names or manufacturers does not constitute and official endorsement, either expressed or implied, by the National Aeronautics and Space Administration.

Three coats of release agent were applied to the tool. The stacks of fabric were cut to dimensions of 10.2 cm x 22.9 cm. The fabric preform was placed on the tool to form a C-shaped part with a web length of 10.2 cm, a flange height of 6.4 cm and a width of 10.2 cm. The preform was oriented on the tool so that the [0] layers were parallel to the resin flow direction (Figure 1a). A 10.2 cm x 27.9 cm layer of Armalon® release cloth was placed on top of the preform. The high permeability distribution media consisted of two 7.6 cm x 26.7 cm layers of Plastinet® nylon mesh. A 1.3 cm gap between the edge of the media and the preform side edges and end (vacuum) edge was maintained. These gaps minimize race tracking of the resin during infusion. A 5 cm length of distribution media was used to place the resin injection spiral tubing. The resin was supplied to the part from the reservoir through 0.9 cm diameter plastic tubing. Likewise, vacuum was drawn on the part through a spiral and plastic tubing (not shown). Figure 1b shows a photograph of the tool-preform assembly prior to the infiltration.

Thermocouples were placed between the two stacks of preform, on the tool surface and on the top of the bag. The lay-up was bagged using a flexible film and silicone bagging tape. The bag and tubing connections were fully evacuated and checked for leaks prior to resin infusion. The system pressure was monitored throughout the process using a vacuum gauge located at the resin trap. Approximately 300g of SI-ZG-5A epoxy resin was prepared and degassed under vacuum for one hour prior to injection. The viscosity of the resin was measured using a Brookfield rheometer and found to be 0.28 Pa·s at room temperature (≈ 25°C).

The resin infiltration was accomplished with the resin pressure set to the atmospheric pressure. The media was rapidly saturated in 20 seconds. The preform was fully impregnated in approximately 60 seconds. To insure complete wetting of the preform, resin was allowed to flow for a total duration of 12 minutes. Then the resin tubing was clamped and the part was kept under full vacuum for an additional 12 minutes. Finally, the vacuum tube was clamped and the part-tool assembly was placed in an oven for cure.

Three cure cycles were used in this study (Table 1). Cycle A followed the resin manufacturer guideline. Cycle B was designed to cure the specimen at low temperature and thus to minimize tool-part interaction. Finally, cycle C was a more aggressive one step cycle with a faster heating rate. After cure, the specimens were debagged and removed from the tool. The specimens were post-cured in a freestanding condition (no tool) for 2 hours at 178°C.

A 2.5 cm wide strip was removed from the C-shaped specimens using a diamond blade saw. Samples were cut from this strip to analyze local fiber volume content as shown in Figure 2. The fiber volume fraction was measured using acid digestion (ASTM D3171-76). Micrographs of the specimens were taken to examine the void content and quality of the parts. The cross-section of the C-shaped specimens was scanned with a digital scanner at a resolution of 600 dpi. The angles were measured using digital image analysis. The spring-in was calculated as the difference between the specimen and the tool angles. Specimen thickness variation was also measured using image analysis.

Results and discussion

Figure 3 shows the part temperature during cure for the three cure cycles. As expected for these thin parts, no exotherm was measured. Viscosity profiles obtained from rheometer tests with the temperature profiles shown in Figure 3 determined that resin gelation occurs at approximately 1.0 hour for part C and 3.7-4.0 hours for parts A and B. Table 2 presents the spring-in measured on the resin injection side ($\Delta\theta_{RES}$), on the vacuum side ($\Delta\theta_{VAC}$) and the average of the two. The largest spring-in was obtained for part C followed by part A and part B. Part B had virtually no spring-in. A significant difference in spring-in between resin and vacuum side was observed in all cases. The resin side spring-in ($\Delta\theta_{RES}$) was 0.89° larger than the vacuum side ($\Delta\theta_{VAC}$) for part A and 0.69° larger for both parts B and C. Figure 4 presents the fiber volume fraction variation in the parts. The average fiber volume fraction was 46.9%, 48.0% and 46.5% for parts A, B and C, respectively. As shown in Figure 4, part B had a more uniform fiber volume fraction distribution compared to parts A and C. Part A had a higher fiber volume fraction on the vacuum side (section 3), while higher fiber volume fraction was found in the web (section 2) for part C. Figure 5 shows the measured thickness variation. In all cases, a corner thinning of 0.2-0.4 mm was found. No significant differences were observed in thickness in the flanges between the resin and vacuum side. Overall, part B was slightly thicker than parts A and C. Micrographic analysis of the sectioned parts revealed a negligible void content and excellent wetting of the fibers.

From the variation in spring-in measured in these experiments it is clear that the cure cycle has a significant effect on the magnitude of part spring-in. In this case, the lowest spring-in was obtained for the cure cycle having the lowest cure temperature (cycle B). If only thermal effects (cool down stresses) are considered, this result is predictable as cycle B has a lower cooling temperature change ($\Delta T \approx 40°C$) than cycles A and C ($\Delta T \approx 100°C$). Thus, cooling residual stresses, caused by a difference in longitudinal and transverse CTE, are greater for part A and C leading to larger spring-in angles. For cycles A and C, the difference in spring-in can be explained by the faster heating rate used in cycle C. During heating and after the

resin gel point has been reached, the mismatch in CTE between the tool and the part led to the development of residual stresses at the tool-part interface. In both of these cycles (A and C), the part-tool assembly is heated after resin gelation occurred. At that stage, the resin is in a viscoelastic state, thus some residual stresses were locked in (elastic) while others relaxed (viscous). A slower heating rate allowed more time for the stresses to relax resulting in lower final residual stresses.

The post-cure also affected the final spring-in angle of the part. As observed on resin transfer molded angles (10), the post-cure cycle in freestanding condition (i.e. without tooling interaction) significantly affects the angle spring-in. Typically, the post-cure is accomplished at a temperature greater than the curing temperature. In the present case, the post-cure temperature was 178°C, while the curing temperature was 66°C for part B and 125°C for parts A and C. Therefore, further cure of the resin takes place during the post-cure cycle. The variation of the spring-in angle with temperature during the post-cure cycle is depicted in Figure 6. Point 1 corresponds to the spring-in angle after the first cure (cycles A-C). During the heating to the post-cure temperature, the part will expand resulting in a decrease in spring-in angle. At the resin glass transition temperature (T_g, point 2), the resin will change from a glassy to a rubbery state. At this stage, any frozen residual stresses will be released resulting in an increase in spring-in (point 2 to 3). At temperatures greater than the resin T_g, the CTE of the resin in the rubbery state is much larger than in the glassy state. Therefore, the spring-in angle will decrease at a higher rate from point 3 to 4. At the post-cure temperature, further cure of the resin will induce chemical cure shrinkage that increases the spring-in angle (point 4 to 5). Finally, during cool down (point 5 to 6), the spring-in will increase to its final value.

It is clear that the cure history can significantly influence the spring-in angle variation during post-cure. The key factors are the resin glass transition temperature obtained after the first cure, the maximum cure temperature and the residual stresses frozen in the part after the first cure. In this study, using a long cure at low temperature (cycle B) led to a low T_g and a low level of residual stresses after cure. All combined, these factors gave the lowest spring-in compared to the other cure cycles. To fully understand the difference between cycles A and C would require a more detailed study of the cure shrinkage and the development of T_g of the resin used.

The difference of spring-in angle between the resin and vacuum side may come from different sources. The obvious one is a difference in tool angle that would necessarily lead to different spring-in angles. The tool angles were measured and the two angles were essentially equal at 90.005°. Another factor would be the variation of thickness at the corner causing a change in the spring-in angle. From Figure 5, it is not clear that a consistent difference exists in the corner thickness between the resin and vacuum side. The final possibility is a difference in resin content between the resin side and vacuum side. From Figure 4, only part A had a significant difference in volume fraction between the resin and vacuum side. With the limited number of samples made in this study, it is difficult to draw any conclusion to explain the difference in spring-in between resin and vacuum side. However, the difference could be induced by the asymmetric flow pattern used to make the C-shaped laminates and the presence of the distribution media.

Conclusion

Void free C-shaped carbon fiber-epoxy laminates were produced using the vacuum assisted resin transfer molding process. The measured part thickness profile showed a small corner thinning typical of sharp corner laminates produced on an open mold. The cure cycle significantly influences the final part spring-in angle. For the resin system studied, a long 66°C cure followed by a 178°C post-cure produced a part with virtually no spring-in (0.05°). A difference in spring-in angle between the resin and vacuum side was more likely caused by the asymmetric flow pattern used to infiltrate the parts.

References

(1) Van Tooren, M.J.L, Dirven, M.P. and Beukers, A., *Journal of Composite Materials*, 35:1, 1587-1603, (2001)

(2) Flin, E.D., *Aerospace America*, July, 33-34, (2001)

(3) Sun, X., Li, S. and Lee, J., *Polymer Composites*, 19:6, 807-817, (1998)

(4) Kang, M.K., Lee, W.I. and Hahn, H.T., *Composites Part A*, 32, 1553-1560, (2001)

(5) Han, K., Jiang, S., Zhang, C. and Wang, B., *Composites Part A*, 31, 79-86, (2000)

(6) Loos A.C., Sayre J.R., McGrane R.D. and Grimsley B.W., *SAMPE International Symposium*, 46, 1049-1060, (2001)

(7) Albert, C., Fernlund, G. and Poursartip, A., *CANCOM 2001*, Montreal, Canada, (2001)

(8) Huang C.K. and Yang S.Y., *Composites Part A*, 28A, 891-893, (1997)

(9) Wiersma H.W., Peeters J.B. and Akkerman, R., *Composites Part A*, 29A, 1333-1342, (1998)

(10) Svanberg J.M. and Holmberg J.A., *Composites Part A*, 32, 827-838, (2001)

Table 1 Cure cycle definitions.

Cycle	Definition
A	Heat to 66°C @ 0.56°C/min Hold 2.5 hours Heat to 125°C @ 0.56°C/min Hold 2.5 hours Cool to RT
B	Heat to 66°C @ 0.56°C/min Hold 13 hours Cool to RT
C	Heat to 125°C @ 1.1°C/min Hold 2.5 hours Cool to RT

Table 2 Parts spring-in measurements.

Part	$\Delta\theta_{RES}$ (°)	$\Delta\theta_{VAC}$ (°)	Average (°)
A	1.09	0.21	0.65
B	0.39	-0.29	0.05
C	1.49	0.81	1.15

RES: resin side

VAC: vacuum side

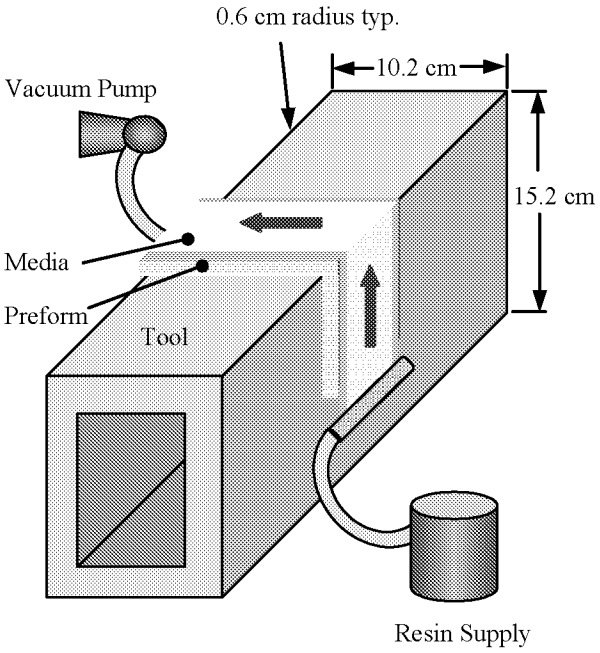

a)

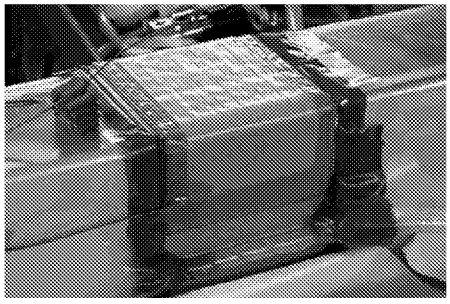

b)

Figure 1 a) Schematic of VARTM setup, b) Photograph of tool-part assembly prior to infiltration.

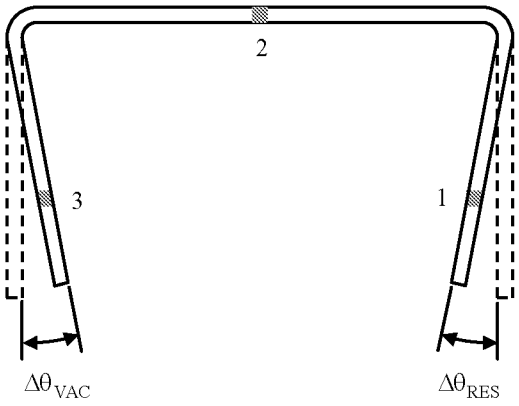

Figure 2 Part measurement points and fiber volume fractions with measured locations (1-3).

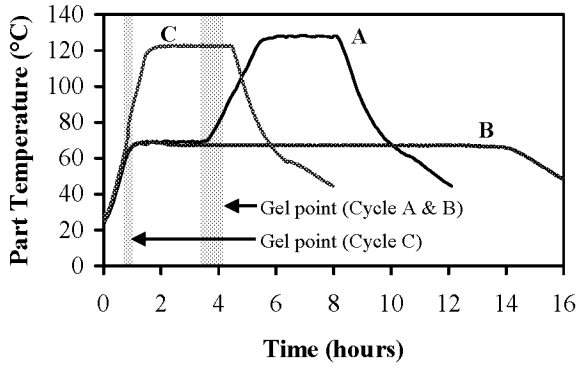

Figure 3 Part temperatures measured during cure and gel point ranges measured with rheometer.

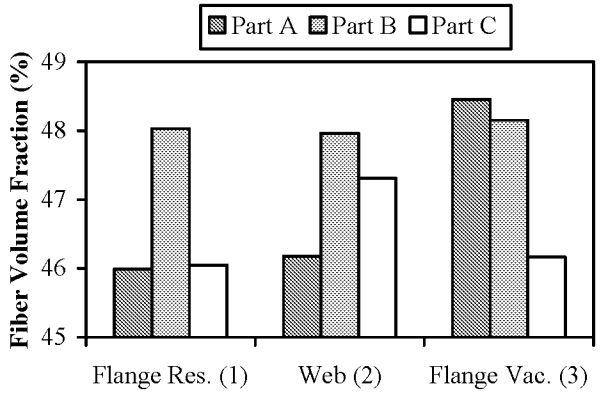

Figure 4 Average fiber volume fraction.

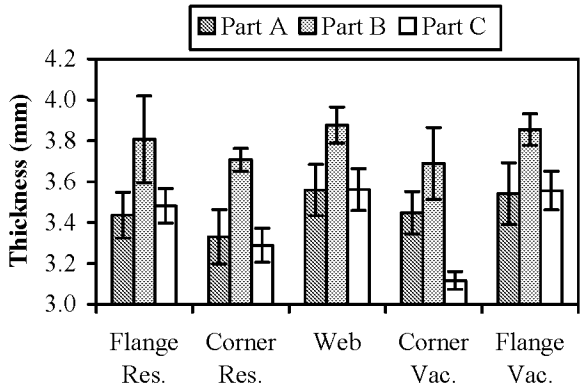

Figure 5 Part thickness variations.

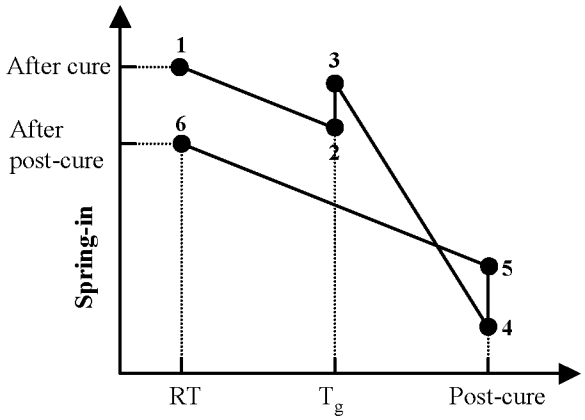

Figure 6 Spring-in variation during post-cure, from (10).